Nature Environment and Pollution Technology
An International Quarterly Scientific Journal

p-ISSN: 0972-6268
(Print copies up to 2016)
e-ISSN: 2395-3454

Vol. 25 | No. 1 | Article ID B4343 | 2026

Original Research Paper

https://doi.org/10.46488/NEPT.2026.v25i01.B4343

Open Access Journal

Sunlight-Induced Photocatalytic Degradation of Methyl Red Using Lignocellulosic Biomass of *Ricinus communis* Stem with Isotherm and Kinetic Modeling

V. Nirmala Devi[1]†, B. Jeyagowri[1], S. J. Pradeeba[1], L. Vidhya[1] and N. Nithiya[2]
[1]Department of Chemistry, Hindusthan College of Engineering and Technology, Coimbatore-641032, India
[2]Department of Physics, Hindusthan College of Engineering and Technology, Coimbatore-641032, India
†Corresponding author: V. Nirmala Devi; keerthi16nir@gmail.com

Abbreviation: Nat. Env. & Poll. Technol.
Website: www.neptjournal.com

Received: 21-04-2025
Revised: 04-06-2025
Accepted: 13-06-2025

Key Words:

Photocatalysis
Ricinus communis stem
Methyl red
Adsorption isotherm
Kinetic studies

Citation for the Paper:

Nirmala Devi, V., Jeyagowri, B., Pradeeba, S. J., Vidhya, L. and Nithiya, N., 2026. Sunlight-induced photocatalytic degradation of methyl red using lignocellulosic biomass of Ricinus communis stem with isotherm and kinetic modeling. *Nature Environment and Pollution Technology*, 25(1), B4343. https://doi.org/10.46488/NEPT.2026.v25i01.B4343

Note: From 2025, the journal has adopted the use of Article IDs in citations instead of traditional consecutive page numbers. Each article is now given individual page ranges starting from page 1.

ABSTRACT

Nowadays, Water pollution is a major global issue brought on by the mixing of effluents from various industries, such as leather, paper, printing, cosmetics, Textile etc., containing metal ions and dyes. This impact causes severe damage to the health of humans, aquatic plants and animals. In view of removing the dyes from the wastewater, several techniques available pose certain drawbacks. To combat such issues, a rapid, cost-effective, eco-friendly, and sludge-less method for removing dye from the effluent using activated *Ricinus communis* stem as a catalyst in the solar irradiation method is discussed and reported with results. The adsorption studies carried out, followed by degradation of methyl red onto Si-RCS, shows 86% in the presence of natural sunlight, and the optimum dye concentration was 20 ppm at 0.25 g photocatalyst dosage. It depicts that the prepared adsorbent material, Si-RCS, can be used as an effective adsorbent as well as a photo-catalyst to treat textile effluents. The best fit model was found to be pseudo-second order based on the R^2 value. Among the isotherm models studied, it was found that Langmuir is the best fit model.

INTRODUCTION

Water is essential to all life for survival. Water pollution is the tainting of bodies of water, including rivers, lakes, ponds, and groundwater, as a result of the dumping of sewage, industrial waste, acid rain, oil pollution, thermal power plants, and eutrophication. One of the most significant industrial sectors involved in environmental degradation is the textile sector. There are 72 hazardous compounds released into water supplies by the dyeing industry, of which 30 hazardous compounds are difficult to remove. Each year, more than 10,000 dyes are used in the textile, leather, paper, rubber, cosmetic, pharmaceutical, plastic, and food industries (Monda 2018). The dye-containing wastewater breaks down into cancer-causing aromatic amines in the absence of dissolved oxygen, which adversely affects the animals, plants, and humans (Jameel et al. 2024). Sludge, industrial waste, and radioactive waste disposal contributes pollutes around 70% of the water resources. Since dyes are typically mutagenic, carcinogenic, and poisonous by nature, industrial effluents should be treated before being released into the environment (Hameed & El-Khaiary 2008).

When aquatic species ingest these textile effluents through the food chain, it can cause several physiological abnormalities, including kidney damage, hypertension, cramps, and occasional fever (Karthikeyan et al. 2006). A risk to survival arises from the buildup of dyes in biotic and abiotic components. Water pollution is a contributing factor to several health issues, including blood disorders, heart conditions, nervous system disorders, skin lesions, vomiting, and diarrhea, including chromosomal changes (Galenda et al. 2014).

Methyl red is a monoazo dye (2-(4-[dimethyl amino] phenyl azo) benzoic acid) used in textile dyeing, paper printing and as an indicator in acid-base titrations. The discharge of Methyl red from various industries causes harmful effects to human beings, plants, animals and the environment (Vinoda et al. 2015). The direct inhalation of methyl red damages the central nervous system, causes digestive system irritation, kidney failure and severe depression, which signifies the removal of methyl red dye before discharging into the environment. Numerous adsorbents were investigated for the removal of Methyl red by various researchers were given in Table 1.

Activated carbon is a widely used adsorbent for the removal of dyes and heavy metals, because it has a large surface area, a high microporous structure, high adsorption capacity, and special surface reactivity (Zhi et al. 2015). Various types of adsorbents are used to increase the degradation capacity in an economic way. Many researchers have attempted to develop adsorbents from various resources such as food waste, agricultural wastes, industrial wastes, etc. (Anjali et al. 2022). Natural materials from agricultural and industrial processes are abundant and could be used as low-cost adsorbents (Mahmoud et al. 2020, Karunakaran & Thamilarasu 2010). Because of their low cost, these materials can be disposed of without requiring costly regeneration after they have been used. Most of the low-cost adsorbents have the limitation of low adsorption capacity, and they generate more solid waste, which poses disposal problems.

The present work investigates the potential of *Ricinus communis* stem activated by silica gel for the degradation of the synthetic textile dye methyl red from wastewater. *Ricinus communis* is a species of flowering plant in the spurge family, Euphorbiaceae, and belongs to a monotypic genus, *Ricinus*, and subtribe, Ricininae (Manickavasagam et al. 2013).

Ricinus communis grows throughout the drier parts and near drainages of India. The annual production of *Ricinus communis* is estimated to be more than 1.0 million tons globally, of which India accounts for 60% of the production (Makeswari & Santhi 2013). The removal of heavy metals and dyes using various parts of *Ricinus communis* is listed in Table 2.

Table 1: Degradation of Methyl red using Nano particles and agricultural waste.

Pollutant	Adsorbent used
Methyl red dye	Silica nanoparticles from rice husk
	Nano Fe_3O_4
	Ag-N-Co doppedZnOnanoparticles
	Tungsten trioxide thin films
	Boron and nitrogen-doped TiO_2.
	Seaweed-mediated zinc oxide Nanoparticles
	Spent oil shale

MATERIALS AND METHODS

Adsorbent Material

The stem of *Ricinus communis* (RCS) was collected near Saravanampatti, Coimbatore District (Tamil Nadu). The adsorbent was thoroughly washed in running tap water to remove dirt and other particulate matter. The washed adsorbent was dried, powdered, and stored in an airtight container for further studies.

Preparation of Adsorbent

Preparation of silica-activated *Ricinus communis* stem (Si-RCS): *Ricinus communis* stem powder is dissolved in water and agitated in a magnetic stirrer for 2 h. Silica is added to the slurry, and agitation is continued for another 1h to attain homogeneity. The whole content is kept in a stable place for 8 h to obtain bubble free mixture. Ethanol and NaOH are added to the mixture and kept aside for 24 h to form the final product. The final product is filtered and dried in a hot air oven at 100° C for 5 h. The dried product is packed in an airtight container for further studies (Madhusudhan et al. 2012).

Preparation of the adsorbate: A stock solution of methyl red (1000 ppm) was prepared separately and diluted to the various required initial concentrations.

Instrumentation

The instruments used for the analysis of adsorbent and photocatalytic behavior are a Digital pH meter, Conductivity

Table 2: Removal of heavy metals and dyes using various parts of *Ricinus communis*.

Pollutant	Precursors	Activating agent
Dyes	Castor bean seed	$ZnCl_2$
	Ricinus communis pericarp	H_2SO_4
	Ricinus communis epicarp	$ZnCl_2$
	Ricinus communis	Citric acid
	Ricinus communis pericarp	H_2SO_4
	Ricinus communis castor leaf powder (CLP)	Dried in a hot air oven for 5 h at 105ºC
Heavy metals	*Ricinus communis* pericarp	H_2SO_4
	Ricinus communis pericarp	H_2SO_4
	Ricinus communis leaves	Tannin gel
	Castor leaf *Ricinus communis* powder	Dried and made to 63-μm particles
	Ricinus communis seed shell	Polypyrrole

bridge cell, Mechanical Bench Shaker, UV, SEM, EDX, XRD, FTIR and HPLC.

Characterization of the Adsorbents

Physico-Chemical Characterization of the Adsorbents

Yield: The yield of the adsorbent in percentage was calculated by using the formula given below

$$Yield(Y) = (M/M_0) \times 100 \quad \ldots(1)$$

Where, M =Mass of the activated adsorbent, M_0=Mass of the adsorbent

Moisture content: About 5 g of the adsorbent was placed in a china dish, weighed, and heated for 6 h at 110±20C. After heating, the dish was cooled in a desiccator and weighed. Heating and cooling were performed every 30 min until there was less than a 5 mg difference between the two subsequent weights.

The moisture content is determined by loss in weight.

$$Moistue\ content\ (\%) = [(M - X)/M] \times 100 \quad \ldots(2)$$

Where M = Mass of the material taken for the analysis(g)

X = Mass of the materials taken after drying(g)

Adsorbent pH: About 0.2 g of the adsorbent was weighed and taken in a 50 mL beaker. Thirty mL of boiled and cooled water, whose pH was adjusted to 7.0, was added and heated to boiling. The first 10 mL of the filtrate was rejected. The remaining filtrate was cooled, and the pH was determined using a digital pH meter.

Zero point charge (pHzpc): About 0.2 g of adsorbent was added to a solution of Sodium nitrate of concentration 0.01M, whose pH was adjusted with 0.1M NaOH and 0.1M HNO_3, and the final pH was measured. The results were plotted with initial pH vs. ΔpH (ΔpH =final pH-initial pH). The pH equals zero yields the pHzpc of the adsorbent.

Iodine Number

Determination of iodine value of the adsorbents: Iodine solution was titrated against sodium thiosulphate (A) and with the sample solution (B).

$$\text{Iodine value} = C \times \text{Conversion factor} \quad \ldots(3)$$

Where C = (B-A)

Surface Acidity and Basicity of the Adsorbent

Acidity: To 0.2 g of adsorbent, 25 mL of 0.5 M NaOH solution is taken in a conical flask, and it is agitated for 10 h in a closed flask. Filter it, and the filtrate is titrated against with 0.05 M HCl. Acidity and Basicity are expressed in 'm'moL.g^{-1}

Basicity: To 0.2 g of adsorbent, 25mL of 0.5 M HCl solution is taken in a conical flask, agitated for 10 h in a closed flask. Filter it, and the filtrate is titrated against with 0.05 M NaOH. Acidity and basicity are expressed in 'm' moles.

Determination of surface group (Boehm titration)

The adsorbent was well mixed with 20 mL of a different base in volumetric standards. About 20 mL of the base was added to a 50 mL conical flask containing the adsorbent. The flask was then sealed and agitated in a shaker for 3 days. The solution was filtered, and 5 mL of each filtrate was titrated with 0.1 M HCl using a water–ethanol solution of methyl red as the indicator.

The number of basic sites was calculated from the amount of HCl reacted with the adsorbent material. Then, the various free acidic groups present were derived using the assumption that NaOH neutralizes carboxyl lactones, Na_2CO_3 neutralizes carboxyl and lactones, and $NaHCO_3$ neutralizes only carboxyl groups, respectively. The results obtained can be expressed in milliequivalents per gram (Balakrishnan & Thiagarajan 2021).

Photocatalytic Studies

Batch-mode adsorption studies for individual samples were carried out to determine the effect of different parameters, such as pH, adsorbent dosage, dye concentration, and contact time. Batch adsorption studies were conducted using 250 mL flasks. The adsorbent and adsorbate solution were separated using Whatman 48 filter paper. The concentration of the dye solution was measured using a UV–VIS spectrophotometer 119. All experiments were duplicated, and only the mean values were reported. The maximum deviation observed was less than ±5% (Alzaydien 2009).

A stock solution of methyl red (1000 ppm) was prepared and diluted to the required initial dye concentrations. Degradation studies were carried out in direct sunlight from March 2017 to May 2018. Batch-mode studies were performed using the required amount of adsorbent for each bottle, to which 50 mL of solution of the required concentration and pH was added, and kept in a shaker for 10 min to obtain a homogeneous mixture. After obtaining the homogeneous mixture, it was exposed to direct sunlight. At regular time intervals, the resulting mixture was filtered using Whatman 48 filter paper, and the final concentration of methyl red dye in the filtrate was estimated by a UV–VIS spectrophotometer 119 at a maximum absorbance of 524 nm.

From the initial and final concentration, the percentage of degradation was calculated by using the following equation.

$$\%\ \text{of Degradation efficiency} = \frac{A_0 - A_t}{A_0} \quad \ldots(4)$$

Where η was the degradation ratio, $A_0$was the initial absorbance of the dye, and A_t was the absorbance of the dye after degradation.

Effect of pH

To analyze the effect of pH on the degradation of dye solutions, 50 mL of a 20 ppm dye solution was adjusted from pH 2 to 9 using 0.1 M HCl and 0.1 M NaOH. The optimum dosage of adsorbent was added and kept in direct sunlight irradiation until equilibrium was reached. After exposure to sunlight, the solution was filtered, and the absorbance was measured using a UV–VIS spectrophotometer 119.

Effect of contact time

For the determination of the rate of dye degradation by the studied adsorbent, 50 mL of a 20 ppm dye solution was analyzed for residual dye concentration at different time intervals. The pH, adsorbent dosage, and adsorbate concentration were kept constant.

Effect of Adsorbate Concentration

The effect of adsorbate concentration was studied by varying the concentration of 50 mL of the dye solution, ranging from 20, 40, 60, 80, 100, 120, and 140 ppm. The equilibrium time and pH were kept constant depending on the dye solution under consideration.

Effect of Adsorbent Dosage

The effect of adsorbent dosage, i.e., the amount of adsorbent, on the degradation of dye was studied at various dosages ranging from 0.05 to 0.35 $g.mL^{-1}$ with 20 ppm dye solution. The equilibrium time and pH were kept constant depending on the dye solution under consideration.

UV-Spectral Studies

The degradation ability of Si-RCS was analyzed for the degradation of methyl red dye, which was confirmed by measuring the absorbance at regular time intervals using a UV–Visible spectrophotometer at a wavelength of 524 nm.

RESULTS AND DISCUSSION

Characterization of the Adsorbents

Physico-chemical Characterization of the Adsorbent

The physicochemical properties of Si-RCS were evaluated and shown in Table 3.

The total phenolic and carboxyl groups present in Si-RCS were 1.32 $m.eq.g^{-1}$. The yield and iodine number provide a measure of surface area or the capacity to adsorb small molecules and are associated with the capacity to adsorb substances with low molecular weight. The pollutant uptake was high when the yield and iodine number were high. The high adsorbent moisture content demands a higher adsorbent load and also reduces the effectiveness of Si-RCS.

Table 3: Physicochemical characteristics of the Si -RCS.

Parameters	Values
Yield %	79.51
Moisture content %	6.22
pH	5.50
Surface acidity [$mmoL.gm^{-1}$]	4.63
Surface basicity [$mmoL.gm^{-1}$]	3.01
pH_{zp}	4.00
Boehm titration [$m.eq.gm^{-1}$] Basic sites	2.47
Phenolic and Carboxylic groups	1.32
Carboxyl groups	0.89
Iodine Number $mg.g^{-1}$	2156.11

The negative charge density on the surface of Si-RCS increases when the zero point charge for the investigated adsorbent is lower than the pH of the solution. Surface acidity and surface basicity values confirmed the presence of negative charge density. The presence of basic and oxygenated acidic surface groups on the adsorbent was determined by Boehm titration.

Surface Characteristics

Scanning electron microscopic spectroscopy

The adsorbent's surface features and properties were examined using scanning electron microscopy (SEM). SEM studies revealed the surface texture and porosity of the adsorbent materials. SEM images of Si-RCS are shown in Fig. 1. The SEM images of Si-RCS show the porous and rough surface of the adsorbent. The rough surface and presence of pores facilitate the adsorption of dye molecules onto the adsorbent.

Energy-Dispersive X-ray Spectroscopy (EDS or EDX)

The fundamental principle is that each element has a unique atomic structure that permits a unique collection of peaks on its X-ray spectrum, which accounts for a major portion of the characteristics of energy-dispersive X-ray spectroscopy.

The confirmation of the existence of elements for the studied adsorbent (Si-RCS) was done by EDX analysis. The elements, percentage mass of elements presented in Si-RCS (before and after degradation), were represented in the Fig. 2, and the values were also summarized in Table 4.

Energy-dispersive X-ray spectra showed the presence of O, Na, C, Ca, K, and Si in the adsorbent. These are known as the principal elements of the adsorbent Si-RCS. The main elements were carbon and oxygen, with carbon content being higher than oxygen in Si-RCS. The presence

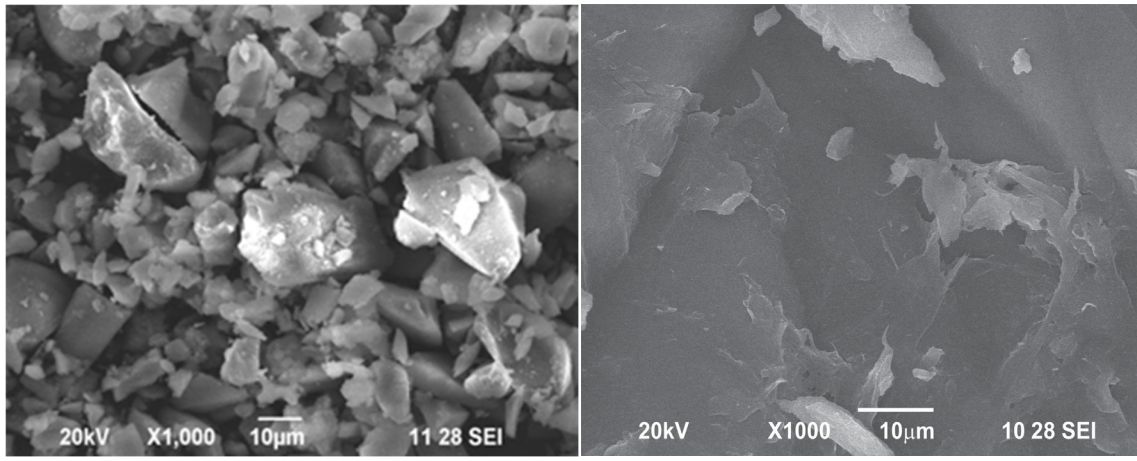

Fig. 1: SEM images of a) Si-RCS and b) Si- RCS after degradation of MR.

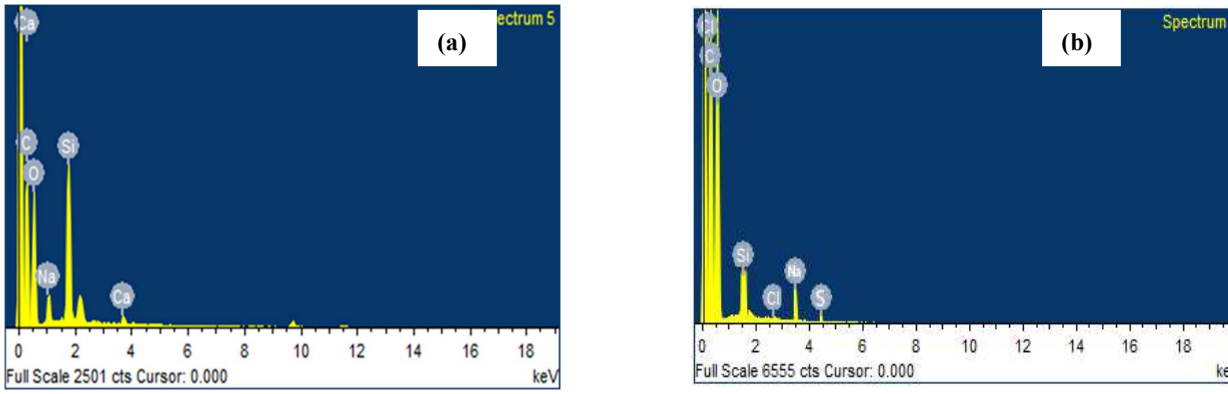

Fig. 2: EDX spectra of (a) Si-RCS and (b) Si-RCS after degradation of MR.

of Si in Si-RCS is attributed to the activation of the RC stem with silica gel.

X-ray Refractive Diffraction (XRD)

The structure of the adsorbent RCS is complex and includes both crystalline and amorphous regions. RCS displays an XRD pattern (Fig. 3a) that is comparable to that of other cellulosic materials. The smallest peak (at around 16° 2θ) denotes a less ordered polysaccharide structure, while the largest peak (at about 22° 2θ) shows the existence of highly organized cellulose.

Fig. 3b shows the XRD pattern of silica-activated RCS. Following silica activation, the crystalline character of RCS was enhanced, as evidenced by the increase in peak intensity in the Si-RCS XRD pattern. However, there are no significant changes in the XRD pattern of Si-RCS after methyl red (MR) degradation.

Table 4: Composition of Si-RCS before and after degradation of MR.

Compound	Si-RCS [Mass %]	Si-RCS-MR [Mass %]
C	25.03	32.75
O	24.62	28.02
Na	3.85	4.77
Si	42.38	10.91
Cl	-	23.47
Ca	4.12	-
S	-	0.08

Fourier Transform and Infrared Spectroscopy (FTIR)

The purpose of employing FTIR analysis was to determine the presence of functional groups with the help of characteristic peaks. Fig. 4a and 4b show the FTIR spectra of RCS and Si-RCS, respectively. The FTIR spectra of Si-RCS exhibit changes in peak intensity and modest peak-position shifts, confirming the silica activation. The FTIR spectra of Si-RCS contain a band at 3171 cm^{-1}, showing the presence of NH groups. A peak at 2878 cm^{-1} indicates

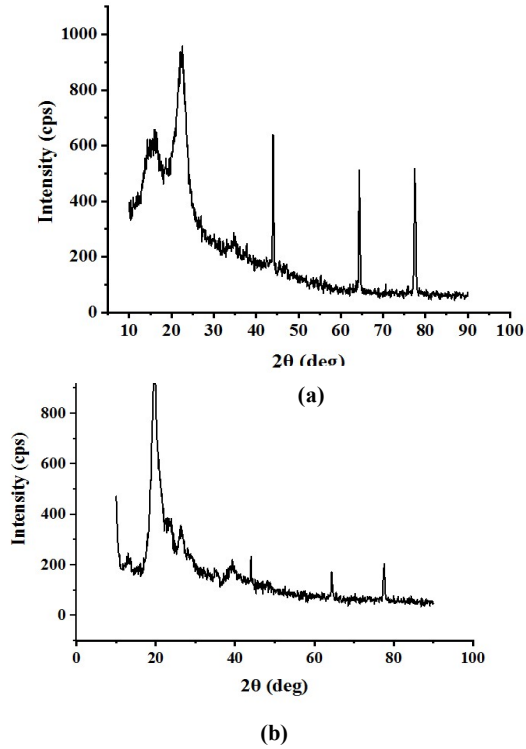

Fig. 3: XRD image of a) RCS and b) Si-RCS.

the presence of symmetric and asymmetric vibrations of methyl and methylene groups. The peak around 2338.82–2353.59 cm^{-1} indicates the presence of C–C stretching due to silica activation. The region at 1505 cm^{-1} is assigned to stretching vibrations of aromatic C=C in lignin, and the peak at 1054.06 cm^{-1} indicates the presence of lignin.

Photo-Catalytic Studies

Effect of Initial Dye Concentration

The effect of the initial dye concentration of methyl red (MR) on Si-RCS was studied using initial dye concentrations ranging from 20 ppm to 140 ppm. The experimental studies indicate a decrease in dye degradation with an increase in dye concentration, as shown in Fig. 5. The degradation efficiencies were found to decline with an increase in the initial concentration of the MR dye solution on Si-RCS. The degradation efficiency of MR onto Si-RCS decreased from 85.85% to 28.98%. The decline in degradation was due to the lack of active sites on the adsorbent surface at higher initial concentrations of MR; the ratio of the initial number of moles of dye molecules to the available adsorption surface area was high. This may also be responsible for an increase in the driving force of the concentration gradient with the rise in initial dye concentration.

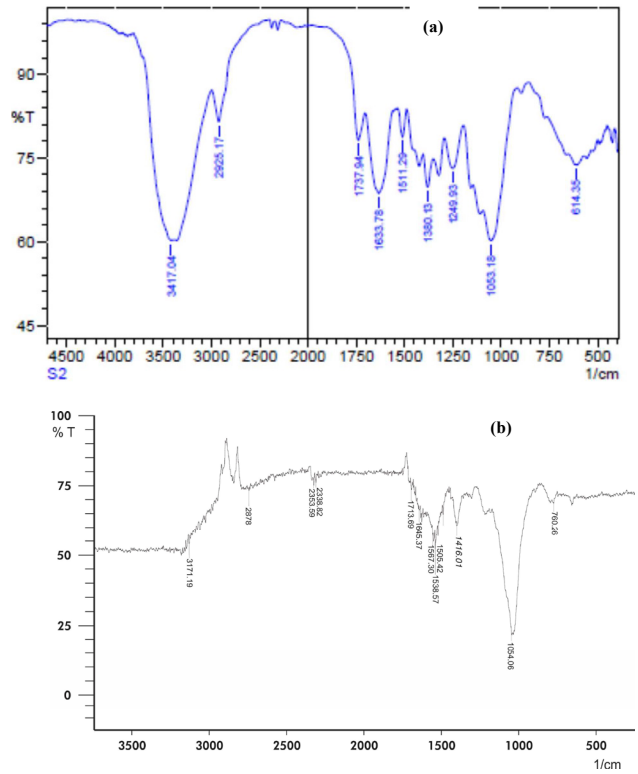

Fig. 4: FTIR image of a) RCS and b) Si-RCS.

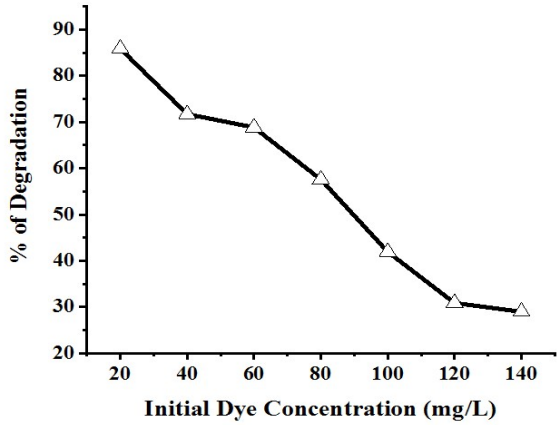

Fig. 5: Effect of Initial Dye concentration on adsorption of MR on Si-RCS.

Effect of Solution pH

The pH of the aqueous dye solution influenced the adsorption process. pH was an important factor that determined the ionizing capability of the adsorbing molecules at the given pH. The effect of the initial pH of the MR dye solution on the amount of adsorption was studied by varying the initial pH of the adsorbent Si-RCS under optimum conditions. The optimum dose of adsorbent was fixed at 0.2 g, 0.25 g, and 0.2 g, and the optimum initial dye concentration was 20 ppm for Si-RCS, respectively. The optimum contact time of Si-RCS was 100 min for the degradation of MR.

The maximum adsorption capacity of the adsorbents with respect to the initial pH of the adsorbate is shown in Fig. 6. The adsorption capacity decreased with increasing solution pH, and the optimum pH value for the adsorption of MR on Si-RCS was 4. The maximum degradation efficiencies of MR on Si-RCS were 80.58% at pH 6 and 85.85% at pH 3, respectively.

Effect of Contact Time

The percentage degradation was found to increase with

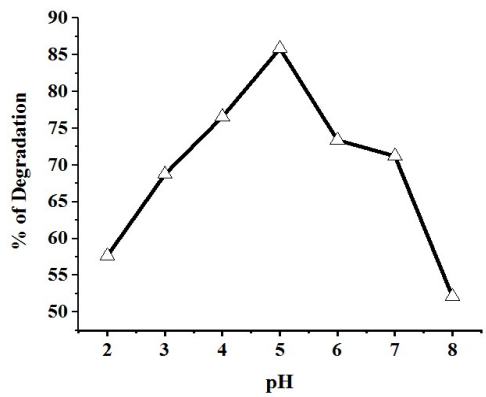

Fig. 6: Effect of pH on the adsorption of MR on Si-RCS.

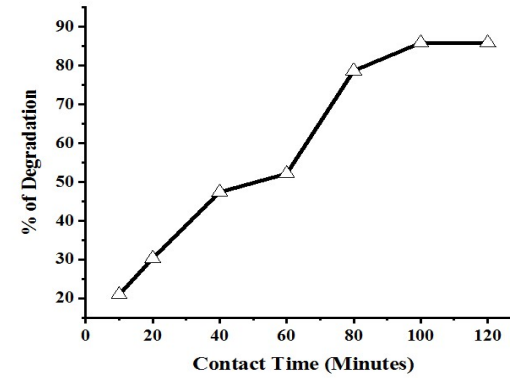

Fig. 7: Effect of Contact time on the adsorption of MR on Si-RCS.

increasing contact time, and then it became stable after attainment of equilibrium time, so the maximum degradation was achieved at 100 min for Si-RCS. This may be because initially the surface of adsorbent sites was highly vacant and the solute concentration was high, and after the equilibrium time, there was no change in the degradation of MR onto the studied adsorbents because the active sites were largely occupied at this stage. The maximum degradation efficiency of MR onto Si-RCS was 85.85% at 100 min. The effect of contact time on the degradation of MR onto Si-RCS is shown in Fig. 7.

Isotherm Modelling

An adsorption isotherm generally explains the dynamic behaviour of any adsorbate from solution to the solid adsorbent phase. The efficiency of an adsorbent for a particular adsorbate removal is represented by adsorption isotherms.

The equilibrium data analysis is important to develop the equation that accurately represents the adsorption process and can be used for design purposes (Balakrishnan & Thiagarajan 2015, 2016). Equilibrium studies determine the adsorption capacities of the adsorbent. To correlate the quantity of adsorption with the liquid-phase concentration, Langmuir, Freundlich, Temkin, and Dubinin–Radushkevich (D–R) adsorption isotherm equations were used. The adsorption isotherm models are evaluated from the values of the correlation regression coefficient (R^2).

Langmuir Isotherm

Irving Langmuir developed the Langmuir isotherm in 1916 to explain the nature of the surface coverage of an adsorbed gas on the surface at constant temperature. The monolayer adsorption on the homogeneous surface of the adsorbent by dye molecules is the main assumption of the Langmuir model (Jeyagowri & Yamuna 2016).

The mathematical expression of the Langmuir adsorption isotherm is:

$$\frac{C_e}{q_e} = \frac{1}{q_{max}} b + \frac{C_e}{q_{max}} \quad \ldots(5)$$

Hence, Ce is the concentration of MR dye solution ($mg.L^{-1}$), qe is the concentration of MR in adsorbent ($mg.g^{-1}$), qmax is the maximum adsorption capacity ($mg.g^{-1}$), and b is the Langmuir equilibrium constant. The linear plot of C_e/q_e vs C_e gives a straight line with a slope of $1/q_{max,}$ and the intercept Ce/qmax is shown in Fig. 8.

The isotherm parameters obtained from the Langmuir model for the removal of MR onto Si-RCS are shown in Table 3. The calculated and experimental values of this model are very close to each other, which indicates a good fit of the parameters to the Langmuir adsorption isotherm model. The correlation regression coefficient is the best evidence that the adsorption of MR onto Si-RCS follows the Langmuir isotherm. The R^2 values for the adsorption of MR onto Si-RCS were 0.991.

Freundlich Isotherm

The Freundlich adsorption isotherm model is a well-known equation used to explain the adsorption process. A Freundlich empirical equation can describe multilayer adsorption and the heterogeneous surface of the adsorbent for non-ideal adsorption. The linear form of the Freundlich isotherm is given as follows:

$$\text{Log } q_e = 1/n \log(C_e) + \log K_f \quad \ldots(6)$$

Where K is the Freundlich constant ($mg.g^{-1}$), n is the Freundlich exponent, q_e is the amount of adsorbed per unit mass of the adsorbent, and C_e is the adsorbate concentration at equilibrium in solution ($mg.L^{-1}$). The Freundlich constant K_f and 1/n were calculated from the slope and intercept from the plot of $\log C_e$ vs $\log q_e$ for the adsorption of MR onto Si-RCS. K_f was approximately an indicator of the adsorption capacity

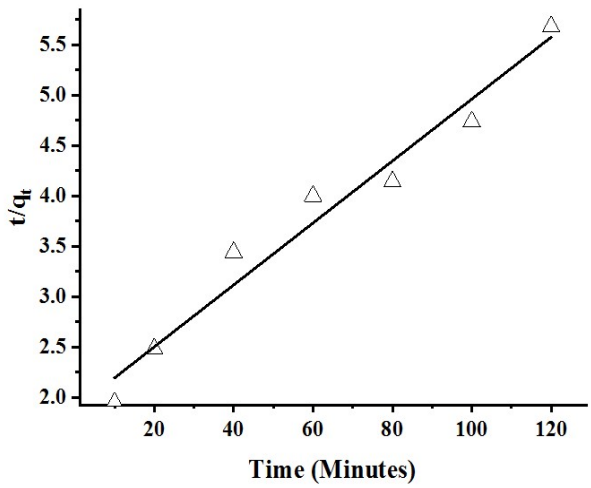

Fig. 8: Langmuir isotherm for adsorption of MR on Si-RCS.

Table 5: Isotherm parameters for the adsorption of MR onto Si-RCS.

Dye		Methyl Red
Langmuir Isotherm	Q_m [$mg.g^{-1}$]	9.58
	b [$L.mg^{-1}$]	3.86
	R^2	0.991
Freundlich Isotherm	K_F[$L.g^{-1}$]	2.912
	N	3.13
	R^2	0.924
Temkin Isotherm	α	0.637
	β	1.94
	R^2	0.905
D-R Isotherm	E [$kJ.moL^{-1}$]	1.000
	R^2	0.9195

related to the bond energy, and 1/n was the intensity of dye adsorption onto the adsorbent surface (Arunachalam et al. 2012). The extent of the exponent, 1/n value, suggested the favourability of the adsorption. The value of 1/n <1 represents a favourable adsorption condition, while 1/n >1 represents cooperative adsorption. The calculated data obtained from the Freundlich adsorption isotherm of the MR onto Si-RCS were summarized in Table 5. The Langmuir and the Freundlich isotherm models were correlated by the regression coefficients (R^2). The correlation coefficient values of MR onto Si-RCS for the Langmuir and the Freundlich isotherms are 0.991 and 0.924. From the results Langmuir adsorption isotherm was well fitted when compared to the Freundlich isotherm model, and confirms the monolayer adsorption of the dye onto the adsorbent (Pradeeba & Sampath 2017).

Temkin adsorption isotherm

Temkin isotherm describes the effect of some indirect adsorbent/adsorbate interactions on the adsorption isotherm indicates that the heat of adsorption decreases linearly with coverage. The simplified form of the Temkin isotherm is as follows:

$$q_e = \beta \ln\alpha + \beta \ln C_e \quad \ldots(7)$$

Where β = (RT)/b, where b is the constant related to heat of adsorption ($L.mg^{-1}$), α is the binding equilibrium constant, T is the absolute temperature (K), R is the universal gas constant (8.314 J), q_e is the amount of adsorbed per unit mass of the adsorbent and C_e is the concentration of the adsorbate in solution at equilibrium condition. The values of α, β and R^2 obtained from the plot of lnCe vs q_e of adsorption of MR onto Si-RCS were presented in Table 5.

Dubinin-Radushkevich Isotherm (D-R isotherm)

The adsorption capacity of the adsorbent is determined by using the Dubinin-Radushkevich Isotherm model. The mathematical expression of the D-R model is given as follows.

$$lnq_e = \boldsymbol{ln\, q_{max} - \beta\varepsilon^2} \quad \ldots(8)$$

Where q_{max} is the theoretical saturation capacity and ε is the Polanyi potential. The constants β and q_{max} can be calculated from the graph plotted between ε^2 vs In q_e for the adsorption of MR onto Si-RCS and are presented in Table 5. The constant β provides the mean free energy *E* of adsorption per molecule of dye when it is transferred to the solid surface of the adsorbent from infinity in the solution. The value of *E* provides information about the nature of adsorption-whether it is physisorption or chemisorption. The adsorption process is physisorption when *E* lies between 1 and 8 kJ.moL^{-1}, while it is chemisorption when is higher than 8 kJ.moL^{-1}. From Table 3, it was observed that the value of *E* is 1.000 kJ.moL^{-1}, confirming that weak physical forces of interaction are the driving force for the adsorption of dye onto Si-RCS (Pradeeba & Sampath 2022a).

From Table 3, it is revealed that the correlation coefficient R^2 of the Freundlich, Temkin, and D–R isotherms were lower than that of the Langmuir adsorption isotherm for the dye, indicating monolayer adsorption of the dye onto the surface of the adsorbent.

Kinetic Modelling

Pseudo-second Order kinetics

The adsorption kinetics of MR onto Si-RCS was explained by using pseudo-second order kinetics. The pseudo-second order equation is:

$$\frac{t}{q_t} = \frac{1}{K_2} - \frac{t}{q_e} \quad \ldots(9)$$

Where K_2 is the equilibrium rate constant for the pseudo-second-order adsorption (g.mg^{-1}.min^{-1}), it can be calculated from the slope of the graph shown in Fig. 9, and the experimental data are summarized in Table 6. The initial adsorption rate and the rate constant k for the pseudo-second-order can be calculated from $h = kq_e^2$ (mg.g^{-1}.min^{-1}) (Vidhya et al. 2023). From the intercept and slope, the values of q_e, k, and h can be determined. The experimental data and the plot were well fitted to the pseudo-second-order kinetic model. The correlation regression coefficient R^2 and the maximum adsorption capacity q_e for the adsorption of MR were 0.9655 and 19.68 mg.g^{-1}, respectively. The calculated q_e values are in good agreement with the experimental data. From the experimental results, it is evident that the adsorption system follows the pseudo-second-order kinetic model and provides a good correlation for the adsorption of MR onto Si-RCS (Mall et al. 2005).

Elovich Equation

The Elovich equation is another rate equation that is typically used to illustrate the adsorption capacity. The equation is exhibited as:

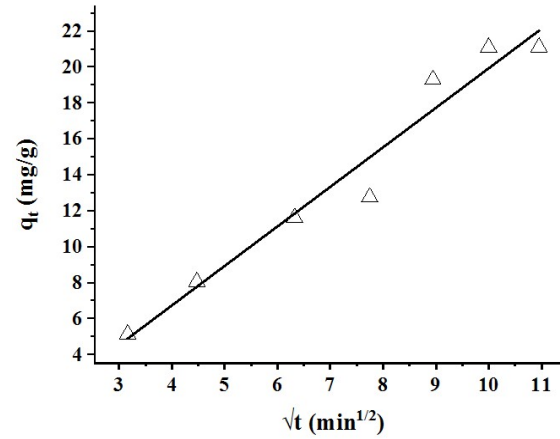

Fig. 9: Pseudo-second order model for the adsorption of MR on Si-RCS.

$$\frac{dq_t}{dt} = B_E \exp(-A_E q_t) \quad \ldots(10)$$

Where A_E is the elution constant (g.mg^{-1}) and B_E is the initial adsorption rate [mg(g.min^{-1})]. A graph is plotted between lnt vs q, and the experimental data were summarized in Table 6. The elution constant A_E and initial adsorption rate B_E for the adsorption of MR were 0.126 and 2.41 for Si-RCS, respectively. The elution constant A_E is lower than the initial adsorption rate, which contributes to the higher adsorption capacity of MR onto Si-RCS.

Intra-particle Diffusion Model

The intra-particle diffusion model is an important tool to find out the mechanism of the adsorption process. The intra-particle diffusion model is expressed as:

$$q_t = K_d t^{1/2} + C \quad \ldots(11)$$

Where C is the intercept, K_d intra particle diffusion rate constant (mg.g^{-1}.min$^{-1/2}$) and q_t is the amount of MR dye adsorbed at time, t(mg,g^{-1}). A plot of qt vs √t gives a linearized form of intra particle diffusion model for the adsorption of MR by Si-RCS, which were studied, and the values were summarized in Table 4. From the results, the intra-particle diffusion rate, K_d, intercept C, and regression correlation coefficient R^2 of MR onto Si-RCS were 2.22 to 2.05 and 0.9593, respectively. The value C (intercept) gives information about the thickness of the boundary layer; if the resistance of the external mass transfer increases, the thickness of the boundary layer also increases (Pradeeba & Sampath 2022b). In the case of intra particle diffusion model, the qt vs √t plots must pass through the origin if the intraparticle diffusion is the rate-limiting step. The plot of qt vs √t for the adsorption of MR by Si-RCS does not pass through the origin, which indicates that the intraparticle diffusion model is not rate limiting step, as surface

Table 6: Kinetic parameters for the adsorption of MR onto Si-RCS.

Dye	Kinetic models	Parameters	Si-RCS
Methyl Red	Pseudo- first order equation	$k_{1[}min^{-1}]$	0.076
		$q_e[mg.g^{-1}]$	14.12
		R^2	0.8233
	Pseudo-Second order equation	$k_2[Lmole^{-1}\ sec^{-1}]$	0.0013
		h	0.503
		q_e,cal$[mg.g^{-1}]$	19.68
		R^2	0.9655
	Elovich Model	$A_E\ [mg.g^{-1}]$	0.126
		$B_E\ [mg.g^{-1}]$	2.41
		R^2	0.911
	Intra-particle diffusion	$k_d\ [mg.g^{-1}]$	2.22
		R^2	0.9593
		C	-2.05

adsorption and intraparticle diffusion were concurrently operating during the dye and adsorbent interaction. The comparison of correlation regression coefficient values for Si-RCS for the adsorption of MR was summarized in Table 6.

The pseudo-second order kinetic model gives a good correlation for all of the adsorption processes of MR onto Si-RCS.

Mechanism of Dye Degradation

The prime reason for using activated *Ricinus communis* Stem as a photocatalyst for the degradation of MR dyes is that when it is exposed to direct solar light irradiation, it gives electron-hole pairs. The dye degradation process is induced by the formed electron hole pairs. Even though it is photocatalytic degradation, initially, adsorption of the dye on the surface of the adsorbent occurs, followed by the photo-degradation process. In the early stages, when the dye concentration is low, there are more vacant sites available on the adsorbent's surface for adsorbing dye molecules; however, as the dye concentration increases, there are fewer vacant sites available on the adsorbent's surface for adsorbing dye molecules. Because the vacant sites are filled by the dye molecules, the rate of dye degradation decreases (Pradeeba et al. 2022). Mechanism of photo degradation occurs in two steps, i.e., Dye adsorption by adsorbent, followed by degradation under direct sunlight takes place by the following equation

$$\text{Adsorbent} + h\nu \rightarrow \text{Adsorbent}\ (e^- + h^+) \quad \ldots(12)$$

$$O_2 + e^- \rightarrow O_2^{\cdot -} \quad \ldots(13)$$

$$O_2^{\cdot -} + e^- + 2H^+ \rightarrow 2OH^{\cdot} \quad \ldots(14)$$

Oxygen plays a vital role in the degradation of dyes.

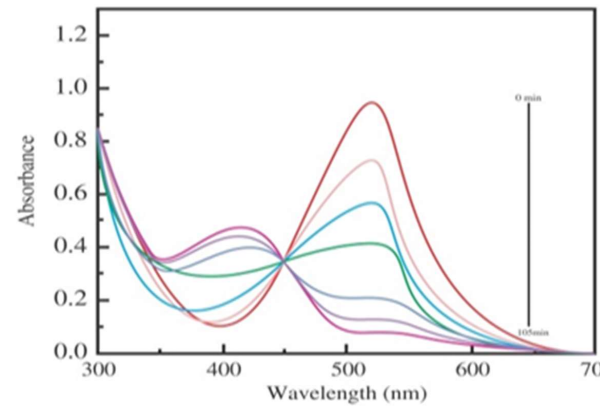

Fig. 10: Photocatalytic degradation of MR on Si-RCS.

The sunlight, oxygen, and hydroxyl ion shows considerable effects on the degradation. The degradation capacity of the dye is reduced if any of the above parameters is reduced. The formed hydroxyl radical species react with any species to form hydrogen peroxide, which is a considerably active species in the photo degradation process. Fig.10 shows the photocatalytic degradation of the dye MR by the adsorbent SiRCS.

$$2OH^{\cdot} \rightarrow H_2O_2 \quad \ldots(15)$$

The formed hydrogen peroxide cleaved to form $OH^{\cdot}$

$$H_2O_2 + h\nu \rightarrow 2OH^{\cdot} \quad \ldots(16)$$

Degradation of dye by $OH^{\cdot}$ radical

$$OH^{\cdot}{}_{ads} + \text{dye} \rightarrow \text{oxidation of the dye} \quad \ldots(17)$$

CONCLUSIONS

In the present research work, silica gel-activated adsorbent was prepared from *Ricinus communis* stem (Si-RCS). The photocatalytic removal of methyl red dye using (Si-RCS) in the presence of natural sunlight was examined. The effectiveness of methyl red dye degradation depends on initial dye concentration, contact time, and pH. In the dye concentration variation, the maximum degradation efficiency was 86% in the presence of natural sunlight, and the optimum dye concentration was 20 ppm at 0.25 g photocatalyst dosage. The adsorbent Si-RCS was utilized as a catalyst in the presence of natural sunlight to investigate the kinetic isotherm, pseudo-first-order, and pseudo-second-order for dye variation. The best fit model was found to be pseudo-second order based on the R^2 value. Adsorption isotherms like the Langmuir and the Freundlich. Temkin and DR isotherm has been analyzed for the dye variation parameter in the removal of Methyl Red. Among the isotherm models studied, it was found that Langmuir is the best fit model.

REFERENCES

Alzaydien, A.S., 2009. Adsorption of methylene blue from aqueous solution onto a low-cost natural Jordanian tripoli. *American Journal of Applied Science*, 6(6), pp.1047-1058. [DOI]

Anjali, K.P., Raghunathan, R., Geetha Devi, and Susmita Dutta, 2022. Photocatalytic degradation of methyl red using seaweed-mediated zinc oxide nanoparticles. *Biocatalysis and Agricultural Biotechnology*, 43, pp.102384-102391. [DOI]

Arunachalam, R., Dhanasingh, S. and Kalimuthu, B. 2012. Phytosynthesis of silver nanoparticles using Coccinia grandis leaf extract and its application in the photocatalytic degradation. *Colloids and Surfaces B: Biointerfaces*, 94(1), pp.226-230. [DOI]

Balakrishnan, J. and Thiagarajan, Y.R., 2015. Biosorption of methylene blue from aqueous solutions by modified mesoporous Simarouba glauca seed shell powder. *Global Nest Journal*, 17(4), pp.701-715. [DOI]

Balakrishnan, J. and Thiagarajan, Y.R., 2016. Potential efficacy of a mesoporous biosorbent *Simarouba glauca* seed shell powder for the removal of malachite green from aqueous solutions. *Desalination and Water Treatment*, 57(24), pp.11326-11336. [DOI]

Balakrishnan, J. and Thiagarajan, Y.R., 2021. Characterization and potential suitability of Simarouba glauca seed shell lignocellulosic biomass as adsorbent of basic dyes from aqueous solutions. *Cellulose Chemistry and Technology*, 55(5-6), pp.705-722. [DOI]

Galenda, A., Crociani, L., El Habra, N., Favaro, M., Natile, M.M. and Rossetto, G., 2014. Effect of reaction conditions on methyl red dye degradation. *Applied Surface Science*, 314, pp.919-926. [DOI]

Hameed, B.H. and El-Khaiary, M.I., 2008. Malachite green adsorption by rattan sawdust: Isotherm, kinetic and mechanism modeling. *Journal of Hazardous Materials*, 159(2-3), pp.574-579. [DOI]

Jameel, R., Lashari, S., Sharif, M.N., Javaid, S., Alam, Faisal Mahmood, F., Ahmad, W. and Kokab, A., 2024. Effective sequestration of Acid Orange-7 dye from wastewater by using *Ricinus communis* biochar along with zinc oxide nanocomposites. *Indus Journal of Bioscience Research*, 2(2), pp.1-20. [DOI]

Karthikeyan, S., Jambulingam, M., Sivakumar, P., Shekhar, A.P. and Krithika, J., 2006. Impacts of textile waste water on fingerlings of fresh water reservoir. *Asian Journal of Chemistry*, 25(16), pp.303-312. [DOI]

Karunakaran, K. and Thamilarasu, P., 2010. Removal of Fe(III) from aqueous solutions using *Ricinus communis* seed shell and polypyrrole coated *Ricinus communis* seed shell activated carbons. *International Journal of Chemtech Research*, 2(1), pp.26-35. [DOI]

Madhusudhan, N., Yogendra, K. and Kittappa M., 2012. Photocatalytic degradation of violet GL2B azo dye by using calcium aluminate nanoparticle in presence of solar light. *Research Journal of Chemical Science*, 2(5), pp.72-77. [DOI]

Mahmoud, N.A., Nassef, E. and Husai, M., 2020. Use of spent oil shale to remove methyl red dye from aqueous solutions. *AIMS Material Science*, 27(3), pp.338-353. [DOI]

Makeswari, M. and Santhi, T., 2013. Removal of malachite green dye from aqueous solutions onto microwave assisted zinc chloride chemical activated epicarp of Ricinus communis. *Journal of Water Resource and Protection*, 5(2), pp.222-234. [DOI]

Mall, I., Srivastava, V.C., Agarwal, N.K. and Mishra, I.M., 2005. Adsorptive removal of malachite green dye from aqueous solution by bagasse fly ash and activated carbon – kinetic study and equilibrium isotherm analyses. *Colloids and Surfaces A: Physicochemical and Engineering Aspects*, 264(1-3), pp.17-28. [DOI]

Manickavasagam, K., Dhanakumar, S., Chandrasekar, P., Narayanan, P.R. and Pattabhi, S., 2013. Removal of reactive yellow from aqueous solution by using *Ricinus communis* pericarp carbon as an adsorbent. *International Journal of Advancement in Life Science Research*, 6, pp.404-416. [DOI]

Monda, S., 2018. Methods of dye removal from dye house effluent: An overview. *Environmental Engineering Science*, 25, pp.383-396. [DOI]

Pradeeba, S.J. and Sampath, K., 2017. Synthesis and characterization of poly(azomethine)/ZnO nanocomposite toward photocatalytic degradation of methylene blue, malachite green, and Bismarck brown. *Journal of Dynamic System, Measurement and Control*, 141(5), 051001-13. [DOI]

Pradeeba, S.J. and Sampath, K., 2022a. Depollution of synthetic dyes from wastewater using polyazomethine/TiO2 and polyazomethine/ZnO nanocomposites via photocatalytic process. *Global Nest Journal*, 24(3), pp.407-413. [DOI]

Pradeeba, S.J. and Sampath, K., 2022b. Photodegradation, thermodynamic and kinetic study of cationic and anionic dyes from effluents using polyazomethine/ZnO and polyazomethine/TiO2 nanocomposites. *Journal of Optoelectronic and Biomedical Materials*, 14(3), pp.89-105. [DOI]

Pradeeba, S.J., Sampath, K. and Jeyagowri, B., 2022. Kinetic and adsorption isotherm modeling of photodegradation of Arunachalamanionic dyes using polyazomethine/titanium dioxide and polyazomethine/zinc oxide nanocomposite. *Desalination and Water Treatment*, pp.262-282. [DOI]

Vidhya, L., Vinodha, S., Pradeeba, S.J., Jeyagowri, B., Nirmaladevi, V. and Nithiya, N., 2023. Adsorption and kinetic studies on the sequestering effect of porous biodegradable biochar obtained from pig-bone on hexavalent chromium from aqueous solution. *Nature Environment and Pollution Technology*, 22(2), pp.681-690. [DOI]

Vinoda, B.M., Vinuth, M., Yadav, D. Bodke. and Manjanna, J., 2015. Photocatalytic degradation of toxic methyl red dye using silica nanoparticles synthesized from rice husk ash. *Journal of Environmental and Analytical Toxicology*, 5(6), pp.1-4. [DOI]

Zhi, L., Lin, C. and Muhammad, A.A.Z., 2015. Metals chloride-activated castor bean residue for methylene blue removal. *Journal of Technology,* 74(7), pp.65-74. [DOI]